Behavior of fused silica materials for microlithography irradiated at 193 nm with low-fluence ArF radiation for tens of billions of pulses

ABSTRACT

R.G. Morton *[a], R.L. Sandstrom [a], G.M. Blumenstock [a], Zsolt Bor [a], C.K. Van Peski [b]
[a] Cymer, Inc., San Diego, CA
[b] International SEMATECH, 2706 Montopolis Dr. Austin, TX 78741

Fused silica samples from seven different suppliers were exposed at low fluence; nominally 0.1 mJ/cm^2, for tens of billions of pulses. These materials are used in the manufacture of projection and other optics needed for DUV microlithography. The fluence level chosen for the exposures was intended to be close to that seen by some of the critical lenses in the projection assembly. Rather than the "compaction" reported by many workers, most of the samples exhibited the opposite effect. The reduction of optical path by DUV radiation or "rarefaction", as we have called it, is a physical phenomenon not known or published previous to our work. Data and experimental conditions are presented which will hopefully lead to the ultimate full understanding of the rarefaction process.

Keywords: Low fluence optical damage phenomena, DUV irradiation, fused silica

1. INTRODUCTION

In a joint project with International Sematech, a facility was constructed at Cymer, Inc., which, through the use of time-delay pulse multiplexing, is capable of illuminating optical material samples at an effective pulse repetition rate of 8 kHz, or four times the 2kHz pulse rate of the line-narrowed Cymer ArF laser used for this project. This arrangement allowed collection of data over a period of several months, which represents 5 to 10 years of field exposure at essentially the same pulse fluence. Attempts to accelerate testing by increasing the fluence to several mJ/cm^2 have been shown by our measurements to be seriously flawed.

Cymer initially irradiated 7 samples of fused silica and 1 of calcium fluoride in order to determine whether these materials could likely last for several years in a stepper optics environment without manifesting significant, or perhaps even measurable compaction. The original 7 fused silica samples were provided to Cymer through Sematech, identified by numbers only. The tests were intentionally blind for all of the usual reasons. Upon receipt of the samples, the Sematech-designated numbers were diamond scribed on the top, left, beam-entrance-end corner to prevent any subsequent errors in ID, or repositioning in the two sample beams following periodic interferometric or birefringence tests. At the 20 billion shot level, some of the samples were no longer yielding meaningful exposure data and so they were replaced with different samples. This can be seen in the plots shown later in this paper.

None of the samples exhibited compaction when exposed to low level fluence. Only two of the fused silica samples showed no change when examined with a phase measuring interferometer (PMI) operating at 633 nm. The rarefaction was measured as a function of dose, and showed no indication of saturation with shot count. The magnitude of the effect, depending on the sample after 40 billion shots was a change of approximately 40 nm out of a sample length of 80 mm , or roughly 0. 5ppm. The calcium fluoride sample showed no measurable changes at all.

The rarefaction result was so astonishing that many checks were made to be sure it was not due to some error in measurement or interpretation of the data. The most convincing proof of its existence came from exposing the same sample to both high

*Correspondence: Email: rmorton@cymer.com; Telephone: 858 385 6309; Fax: 858 385 5353

In *Optical Microlithography XIII*, Christopher J. Progler, Editor, Proceedings of SPIE Vol. 4000 (2000) • 0277-786X/00/$15.00

(3mJ/ cm^2) and low (0.1mJ/ cm^2) fluence pulses in side by side locations within the sample. This was repeated for a second sample with the same result. Phase sensitive interferometric measurements encompassing both areas of exposure showed clearly that the low fluence phenomenon had the opposite sign to the high fluence, better known, compaction. Further, the rarefaction is not a surface effect since it can be seen with a PMI transverse to the direction of the illuminating beam as well as viewing in the beam direction. No surface effect was detectable in the samples.

All of the irradiated fused silica samples exhibited induced birefringence; even the ones that did not show any change when examined with the PMI. Of greater interest are the facts that the nature of the birefringence in the low fluence paths was distinctly different than that seen in the high fluence paths, and that the birefringence in both cases is anisotropic, seemingly due to the linear polarization of the irradiating pulses.

2. EXPERIMENTAL DETAILS

Automated, periodic measurements of the pulse energy, integral-square pulse-width, multiple power head calibrations to a reference power head (which was sent to NIST for absolute calibration) and beam profiles on the samples were used to accurately determine the dose delivered to each sample. This was accomplished using a PC-based data acquisition and control system. The database from this project is very large, and is stored in multiple formats for future rigorous analysis if required.

The basic philosophy behind our detection scheme was that the detectors themselves would only be exposed to 193nm radiation when measurements were being taken. This was intended to minimize any response changes over the several-month run times for which they were used. The detectors were: Molectron, Inc # PM10-19A, with on-board trans-impedance amplifiers, with a nominal output sensitivity of 1 Volt per Watt for measuring fluence; fast photodiodes for recording optical pulse waveforms which were subsequently converted to integral square pulsewidths ($\tau$is) for all 4 pulses in each burst generated by the delay optics for each laser pulse; and a CCD camera with fluorescent converter to record beam profiles for all 4 pulses for both beam lines.

Figure 1 shows a conceptual scheme for producing 4, cleanly temporally spaced pulses for each pulse delivered from a source laser. Because of the large delay times, up to 150ns, implementation of this scheme in practice is quite complex.

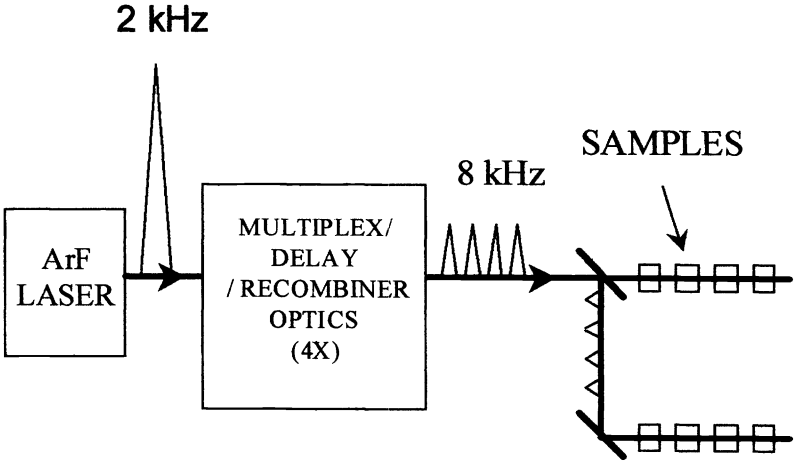

Figure 1. Schematic for Sematech materials life test at 193nm.*

Figure 2 shows a more detailed layout of the optical system used to produce pulse sets. Not only are multiple bounces from dielectric mirrors required in order to introduce the necessary pulse delays, but image relay lenses are also needed to defeat the divergence of the ArF laser beam , which is rather spatially incoherent (something lithographers like , but constructors of long-path optical delay lines do not). The samples and delay table optics were enclosed and purged with dry nitrogen such that the oxygen concentration never exceeded 60 ppm, and were usually less than that level.

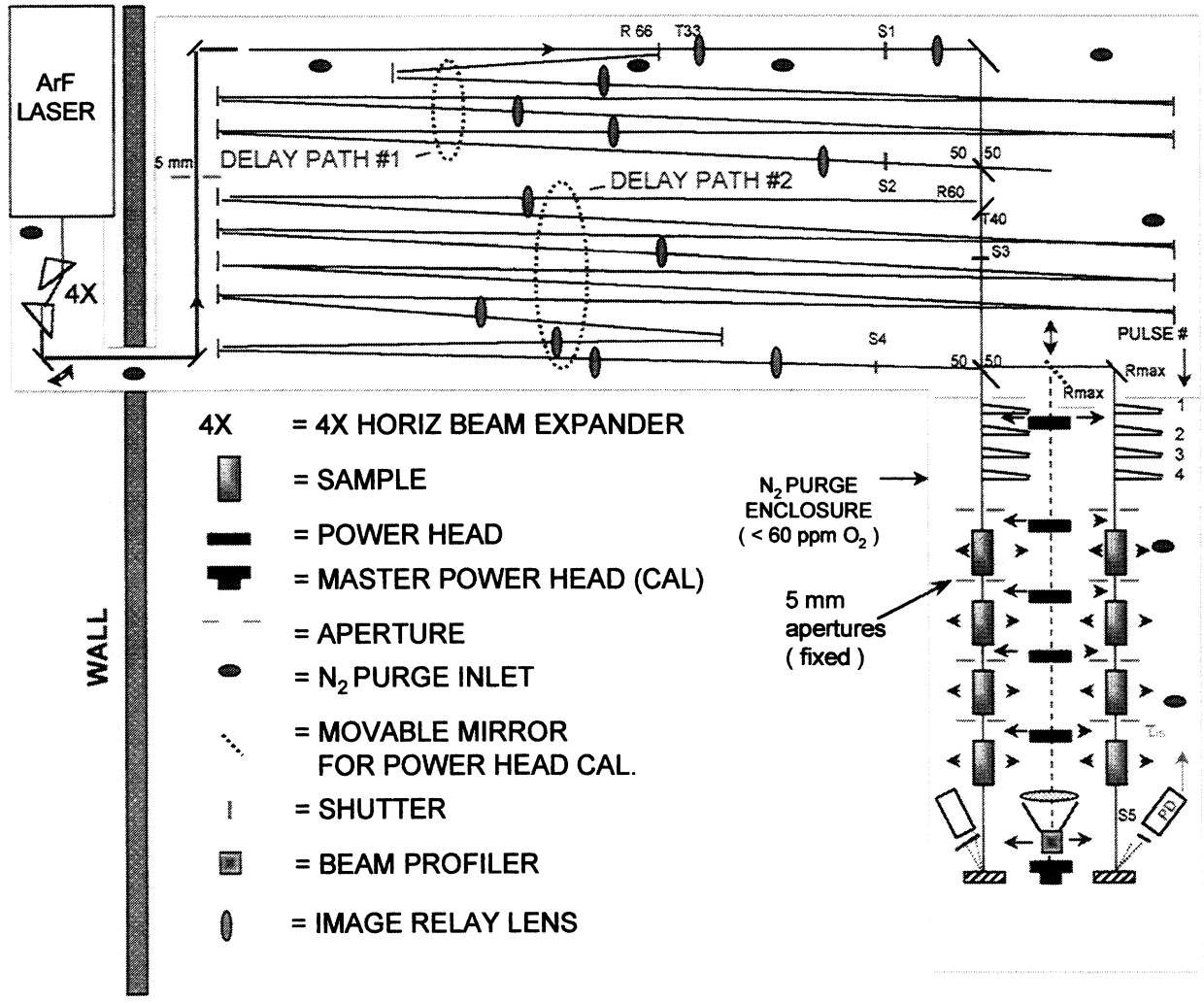

Figure 2. More detailed view of pulse multiplexing and sample exposure configuration.

A 5mm diameter primary, or entrance aperture is imaged onto 5mm apertures at the sample locations. This gives a well defined beam diameter in the samples. Additional 5mm apertures in front of each sample ensure that the beams have essentially the same spatial definition in each sample. The additional apertures cost power but they reject diffracted and over-divergent light from the first aperture in each beam line, thus providing for crisply defined, nearly identical beams in all samples. The first pulse arrives via the shortest path , as can be seen in Figure 2. Beam splitters are used to pick off light for delay paths#1 and #2. Delay path #2 is twice as long as delay path #1 which results in 4 equally spaced pulses with clean temporal separation. Each of the 4 possible paths that the light can take has its own set of image relay optics. Partially reflecting beam recombiners are adjusted to make the 4 beams co-linear at the sample apertures; overlapped in space and pointing angle, but no longer time.

Figure 3 shows the optical pulse waveforms for each of the two beam lines as produced by the multiplexing optical table. The pulse spacing is about 50ns , with the 4th trailing the 1st by 150 ns. Since the laser had sufficient output power to drive two beam lines , each with 4 samples in series , a 50/50 beam splitter / combiner (which is required even for one beam line) gave the opportunity to set up two parallel beam lines. By default, this allowed twice as many samples to be evaluated as were being considered during the initial project planning phase. (In fact, the system could have been configured to produce 4 beam lines since there is another 50/50 beam recombiner at the end of the first delay line. This was beyond the scope of the project, and therefore not done.) The pulse burst shown in Figure 3 repeats every 0.5ms.

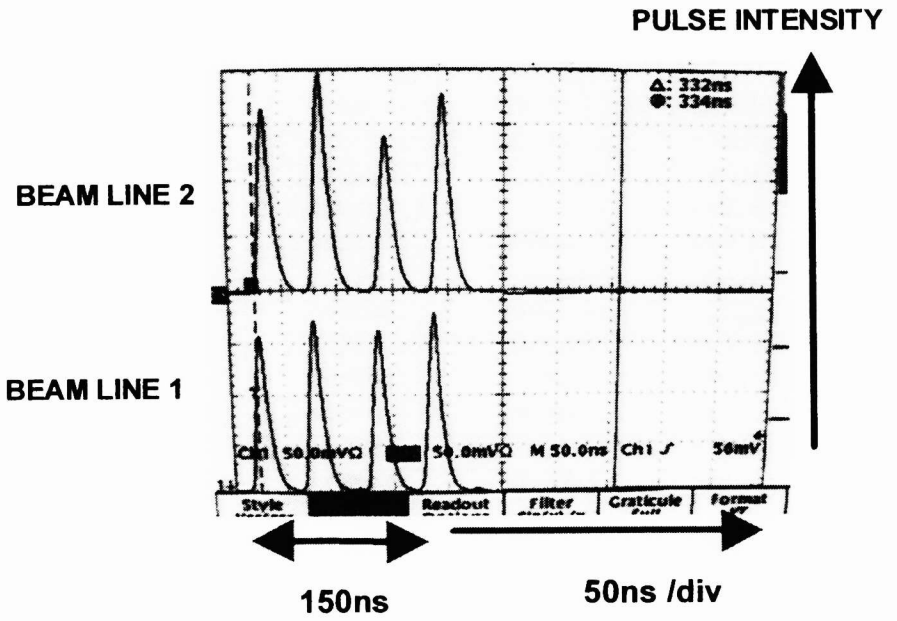

Figure 3. Pulse waveforms for sample irradiation

Referring to Figure 2 again, the method of recording incident power , beam profiles , and on-line absorption for the samples is to use pneumatically (same dry N_2 as purge gas) driven slides to position the power heads , samples and beam profiler camera. Another feature of the system is the ability to record beam profiles for the 4 individual pulses by using solenoid driven shutters and on the delay table. Sufficient data has been acquired to precisely compute the dose for each sample as a function of position within the 5mm diameter illuminated zone. In order to obtain accurate values for the compaction doses delivered to the 8 samples, 5 active power heads and one fixed power head were used. The fixed, or reference, power head is only used to periodically compare the relative responses of the 5 power heads to the same beam and to the reference head.

A power calibration sequence consists of exposing the reference head for 10 seconds, then each of the five active heads , also for ten seconds , then a final exposure of the reference head again. For this calibration a mirror on the delay table is automatically slid into position to deliver a beam running between the two sample-beam lines. Also , the profile camera is slid out of the way to allow exposure of the main , reference power meter head. The two reference head readings are averaged to account for any general drift that may have occurred during the minute or so it takes to complete data acquisition; for instance room temperature; although the sample table is relatively well shielded from such for several minute time periods. The column headings in Table 1 have the form "PMX/REFAVERAGE". The X is just the number of the power head, and the "REFAVERAGE" refers to the averaging of the two reference power head readings as described above.

Table 1 shows the calibration results from 20 different power head measurements made over the course of the first 20 billion shots. Differences in response on any given power calibration test are in the percent range and show no systematic drift among the 5 power heads. Averaging the responses ratioed to the reference head over the 20 measurements shows a difference in the 5 heads spanning a total range of 4 %. As small as the differences are, the responses of each power head were factored into the computation of DUV dose for each sample.

TABLE 1 POWER METER

CALIBRATIONS AMONG THE 5 POWER METERS AND THE REFERENCE* POWER METER

PM1/REFAVERAG	PM2/REFAVERAG	PM3/REFAVERAG	PM4/REFAVERAG	PM5/REFAVERAG
0.956928839	1.009363296	1.009363296	1.02247191	0.970037453
0.961016949	1.03220339	0.996610169	1.008474576	0.972881356
0.867671692	0.984924623	0.984924623	1.020100503	1.078726968
1.015065913	0.975517891	1.054613936	0.975517891	0.962335217
0.986577181	1.010067114	0.986577181	1.010067114	0.963087248
0.986577181	1.021812081	1.010067114	0.998322148	0.974832215
0.958132045	1.025764895	1.003220612	1.014492754	0.980676329
0.954022989	1.034482759	1	1.011494253	0.988505747
0.973913043	1.014492754	1.014492754	1.034782609	0.953623188
0.969879518	1.03313253	0.990963855	1.012048193	0.969879518
0.965517241	1.00265252	1.021220159	1.021220159	0.984084881
0.969639469	1.009487666	1.009487666	1.022770398	0.969639469
0.967370441	1.021113244	1.007677543	1.007677543	0.980806142
0.971530249	1.008896797	1.008896797	1.021352313	0.983985765
0.979123173	1.022964509	1.008350731	1.022964509	0.949895616
0.969450102	0.99796334	0.99796334	1.026476578	0.955193483
0.9625	1.00625	1.020833333	1.00625	0.991666667
0.968421053	1.021052632	1.021052632	1.010526316	0.968421053
0.961661342	1.017571885	1.028753994	1.017571885	0.97284345
0.93987976	1.01002004	1.038076152	0.995991984	0.925851703
PM1RESPONSEAv	PM2RESPONSEAv	PM3RESPONSEAv	PM4RESPONSEAv	PM5RESPONSEAv
0.964243909	1.012986698	1.010657294	1.013028682	0.974848673

Table 1. Power Meter Calibration Data

Figure 4 shows a typical beam profile. Although it is not a pure top-hat distribution, it is recorded and can be used to generate spatial variations in dose within each sample. The dose values reported in this paper are averaged over the entire 5mm aperture.
The profile shown above, in Figure 4, is typical. All beam profiles were stored and are available for post-analysis.

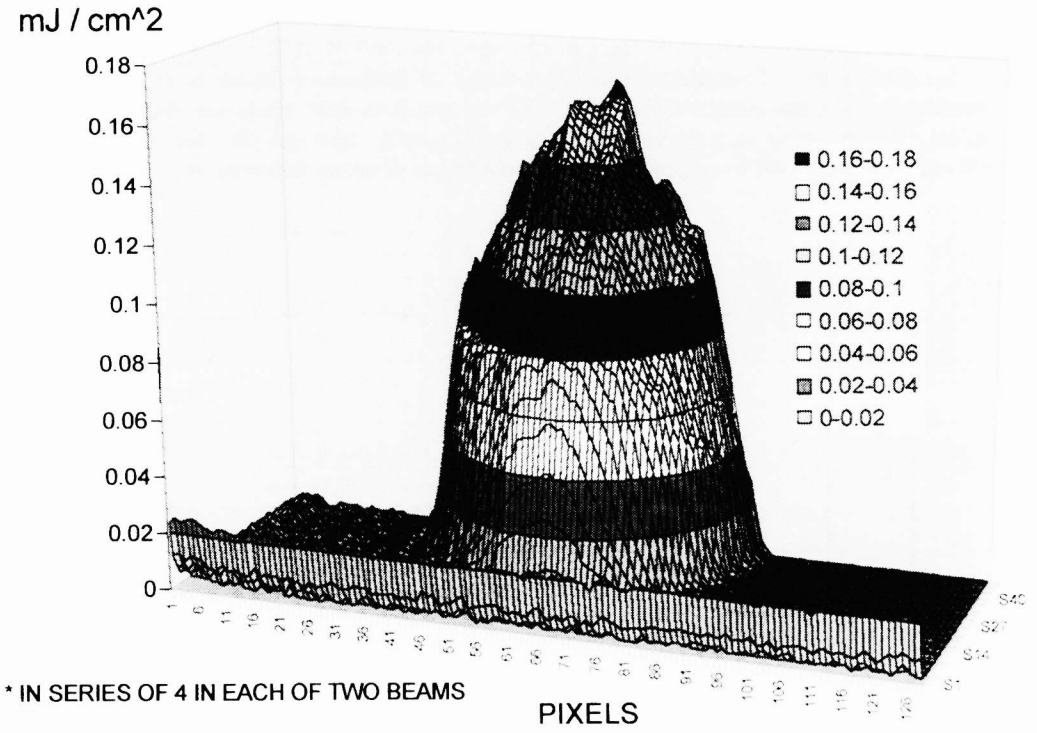

Figure 4. Typical beam profile irradiating samples. Zero cuttoff is 5mm diameter due to hard apertures in front of each of the 8 samples.

DOSE DATA

Figures 5 & 6 show the running integral of the dose delivered to each of 8 samples over the course of the first 40 billion shot run. The units are $10^6((mJ/cm^2)^2)/ns$ according to the Sandstrom definition of integral square pulsewidth as it pertains to compaction dose:

$$t_{IS} = \frac{\left(\int T(t)dt\right)^2}{\int T^2(t)dt}$$

Slope changes indicate differences in delivered laser power over those periods, caused by many different conditions in the delay table optics as well as any inherent change in laser output power. For instance, relatively flat zones may indicate damage to AR coatings on image relay lenses in the middle of the night. **Other problems were encountered as well , but the point is that whatever happened is recorded.** Power levels , energy distribution among the 4 generated pulses , beam profiles for each of the pulses, etc. All of this data has been used to compute the running integral of doses delivered to all of the samples.

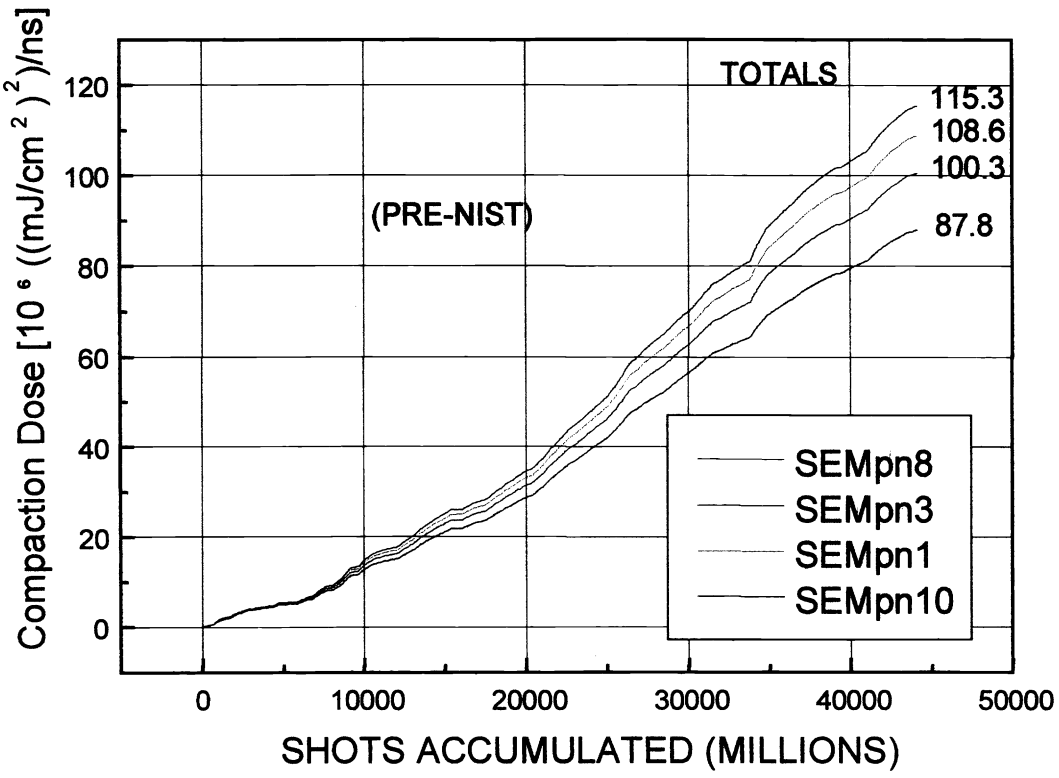

Figure 5. Beamline #1 Doses.

A spreadsheet was used for computing the dose for each sample for each of the 4 pulses produced by the delay table optics. The array which contains the dose data is 32 columns wide by 442 rows just for the initial 20 billion shot run. Data was taken mostly at intervals around 45 to 100 Mshots. The sample doses computed for each interval contain the pulse energy , the number of shots for which that pulse energy was run and the integral square pulse-width during that same interval. Each type of measurement was taken with about 10 second averaging except for the beam profiles which required only a single frame to average (sum) the few tens of pulses occurring within a single CCD camera frame time.

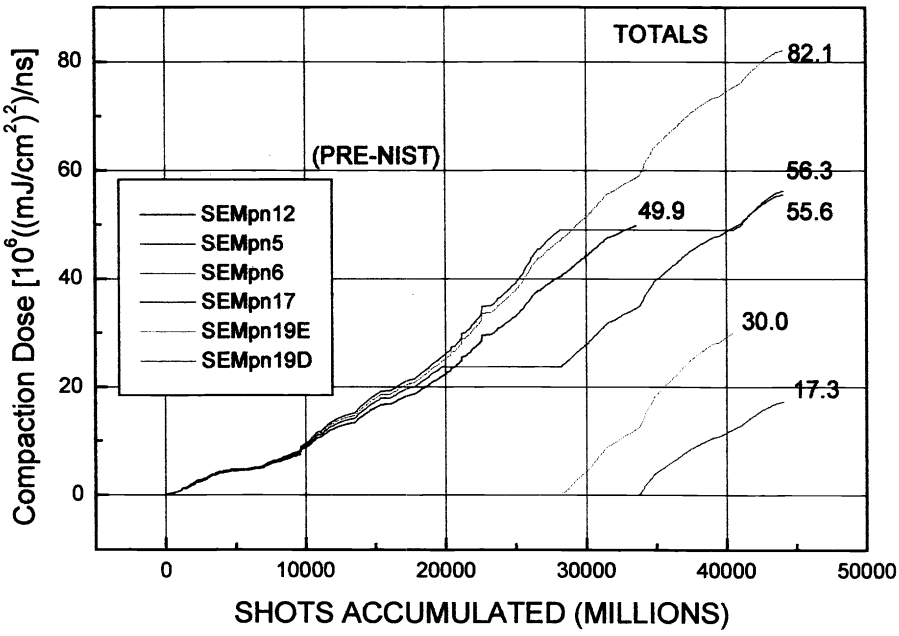

Figure 6. Beam Line #2 doses.

Table 2 lists the total compaction doses delivered to each sample and the qualitative compaction result after 40 billion shots of exposure. Actual compaction values are presented in the following section on interferometric measurements.

As is evident in Table 2 , only two of the 7 fused silica samples showed no measurable optical path changes after exposure , down to the 5nm or 60 ppb in the 8 cm samples. All of the samples were 2 cm x 4cm x 8cm. The beams were directed through the central part of the 2cm x 4cm faces with propagation in the 8 cm direction.

SEMATECH SAMPLE #	DOSE $10^6((mJ/cm^2)^2)$/ns	COMPACTION
10	115.3	"de-compaction"
1	108.6	zero
3	100.3	"de-compaction"
8	87.8	"de-compaction"
17	56.3	zero
6	82.1	"de-compaction"
5	55.6	"de-compaction"
12	49.9	Zero (CaF_2)
19E	30.0	"de-compaction"
19D	17.3	"de-compaction"

Table 2. Total compaction doses and results.

Interferometric Data

Table 3 shows the actual amounts of compaction for each sample.

Sample #	1	3	5	6	8	10	12	17	19D	19E
Shot Count (B)	Approximate Measured Compaction (nm)*									
0	0	0	0	0	0	0	0	0	0	0
1.65	0	0	0	0	0	0	0	0	--	--
3.126	0	0	0	0	0	0	0	0	--	--
7.182	--	--	--	--	--	--	--	--	--	-10
10.11	0	0	0	0	0	-8	0	0	--	--
10.72	--	--	--	--	--	--	--	--	-11	--
11.69	0	-6.2	0	-5	-4	-10	0	0	--	--
15.142	0	-13	0	-12	-6	-15	0	0	--	--
20.038	0	-17.5	-14	-14	-10	-20	0	0	--	--
22	--	--	-20	--	--	--	--	--	--	--
29.462	0	-29	--	-22	-22	-30	0	0	--	--
32	--	--	-28	--	--	--	--	--	--	--
40.182	0	-42	--	-37	-33	-40	--	--	--	--

* Peak value in central zone.

Table 3. Measured compaction.

A # MK4 phase-sensitive Zygo, Inc. interferometer ("Zygo") using a HeNe light source was loaned to Cymer by Sematech for the purpose of making measurements on the samples provided. The samples were exposed with the beam running at a ½ degree angle with respect to the end face normals. The samples were mounted at this same ½ degree angle for measurements in the Zygo so that there would be no interference patterns arising from the sample faces and so that the double pass viewing angle would be the same as the exposure angle. Otherwise, the circular exposed regions would have a slight elliptical distortion imposed on them.

Although vast amounts of interferometric data are available, the data presented here for a single sample reveals the existence of the recently discovered phenomenon of "rarefaction" that occurs at low fluence. At fluences of a few mJ/cm2 many workers have observed the "compaction" or increased density and therefore optical path after prolonged exposures; about 50 million shots. The scaling laws for compaction have been worked out and presented elsewhere in the literature. What was not expected was that at "low" fluence , less than about 0.2mJ/cm , another physical mechanism dominates such that the optical path is reduced.

Figures 7 and 8 illustrate the two effects, compaction and rarefaction, occurring in the same piece of material. Although the figure shows the result for one particular sample (#10) the same result was seen in sample #6. No other samples were exposed at high fluence due to the constraints of time associated with accumulating 40 billion pulses at low fluence on many samples. Note that in the interferograms the sign of the optical path difference is opposite to that normally displayed. This was done deliberately because we were expecting to see compaction, if anything, and it is easier to visualize 3-d distributions of the "hill" type than the "valley" type of plot.

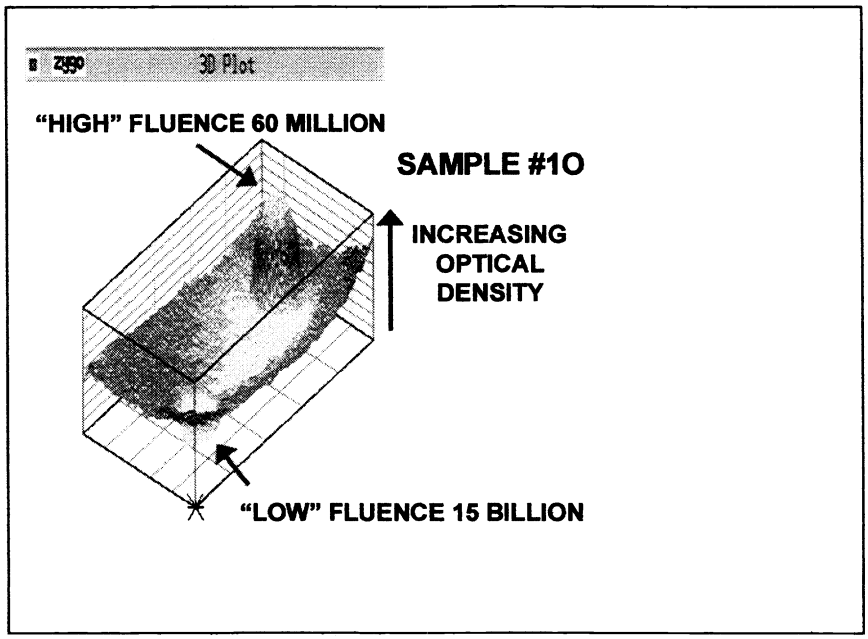

Figure 7. Showing compaction and rarefaction in the same fuse silica sample.

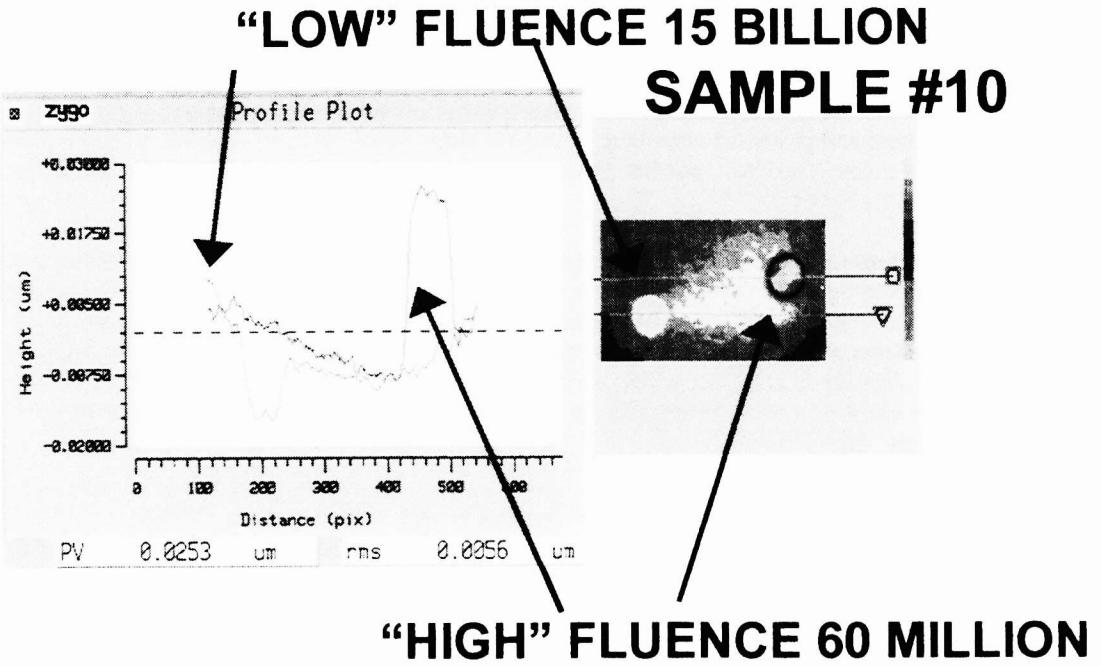

Figure 8. Cross sectional measurements of the high and low fluence zones.

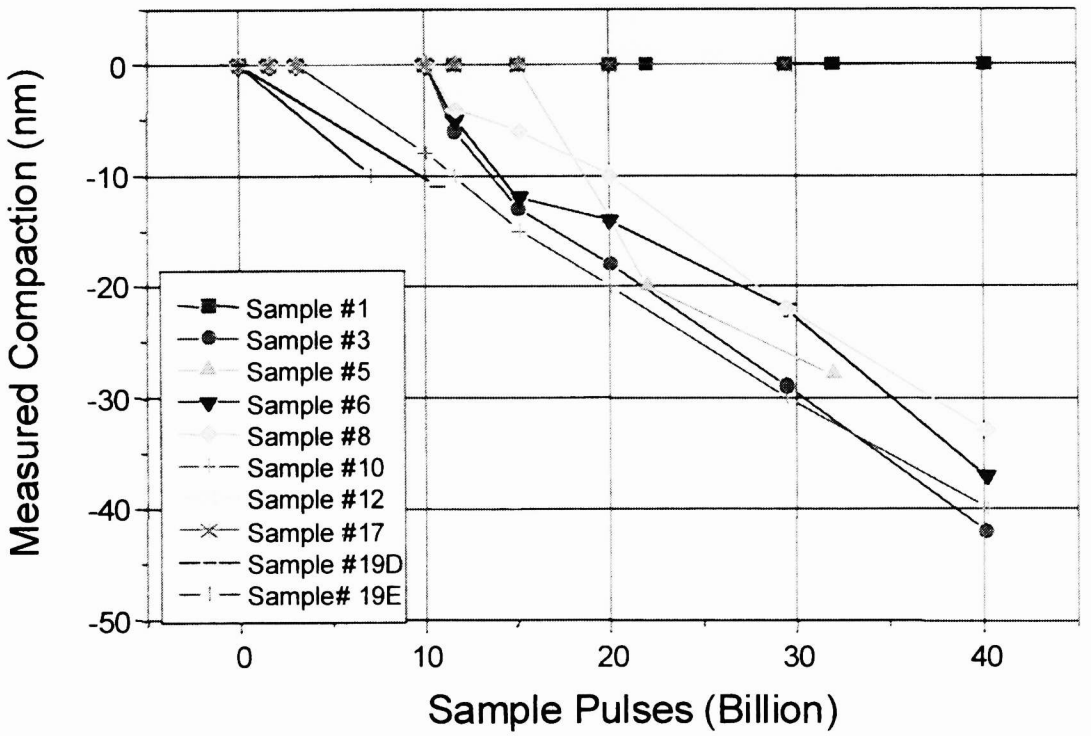

Figure 9. Compaction as a function of shot count.

ABSORPTION

One of the purposes of the Sematech Phase2 study was to make on-line absorption measurements. The idea was to read the power on the meter immediately behind a sample and then to slide the sample out of the beam path and repeat the power reading. Subtraction of known Fresnel losses would then yield the internal absorption loss and track changes in this quantity.

It was not possible to make accurate absorption measurements with our initial set–up because the noise on the laser power was more than 1% on the time scale of a typical absorption sequence, and because we had no reference detector to compensate for the fluctuations.(It should be pointed out that 1% laser noise is not a problem in recording exposure data , because it averages out to a much smaller value over very long time periods and over 442 measurements. It is a problem when the absorption is of the same magnitude as the noise, however). The sample materials provided have much lower absorption than any we have encountered in the past. There were also questions about surface contamination when the samples were removed from their nitrogen purged enclosure for off-line absorption tests

A new method for making on-line absorption measurements was implemented after the first 20 billion shots of exposure on the samples. The protocol was changed so that a second power head acted as a reference in order to subtract out any variations in laser power occurring during the period of the absorption measurements. This worked very well, as can be seen in Figure 10.

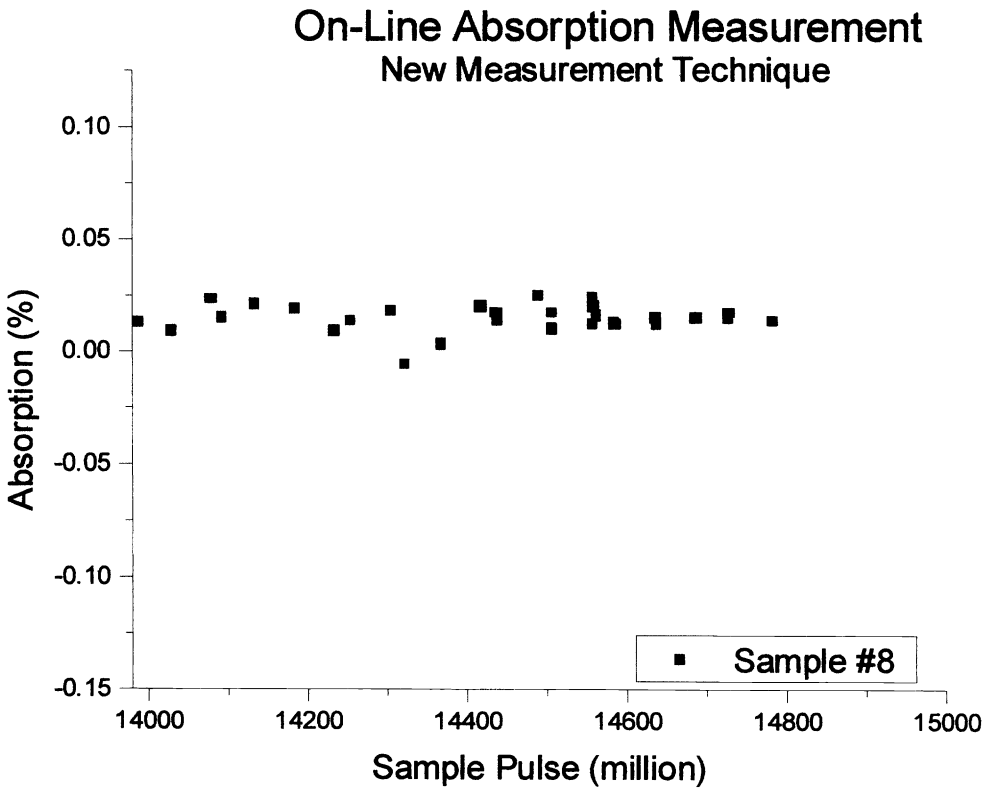

Figure 10. Showing greatly improved measurement accuracy using modified on-line method.

The absorption measurement accuracy was reduced from 1% to about 0.02% using this method, and there were no questions about surface contamination or delay time between end of exposure and the external measurement encountered with the original method.

3. BIREFRINGENCE MEASUREMENTS

Birefringence measurements were made using a Hinds Instrument: Exicor 620. This instrument is capable of mapping the sample and providing both magnitude and direction of the birefringence over a selected grid. Birefringence maps of samples 10 and 17 are shown in Figs 11 and 12, respectively. Sample 17, shown in fig. 11, was chosen because it is one of the two samples that show little or no wavefront distortion. Sample 10 was chosen because it has the highest rarefaction at low level irradiation and also, is one of the samples irradiated in a separate area with 100 million pulses at $3mJ/cm^2$.

Two observations are noteworthy from these birefringence measurements. First, for sample 10, on the high level of irradiation spot, the birefringence magnitude is peaked in an annulus around the periphery of the irradiated area, and the vectors are generally tangential to the annulus. This is as expected from a uniformly compacted cylindrical volume. The exposed area that received low level irradiation has a birefringence magnitude that peaks in an elliptical-shaped spot. The birefringence vectors are perpendicular to the major axis of the spot. This is typical for all of the low fluence regions of all of the samples.

We do not yet know the mechanism of the refractive index reduction at low level ($< \sim 0.2\ mJ/cm^2$) exposure, but it is obviously related to absorption (one or multiphoton) of the linearly polarized exposing laser light. Therefore it is reasonable to expect an anisotropic refractive index change.

The second observation of interest is that although the birefringence of the low-level irradiated areas of sample 10 and 17 are almost identical, the wavefront distortion (i.e. rerefaction) of the two samples differs by at least an order of magnitude. Sample 10 shows 30nm rarefaction, and the rarefaction of sample 17 is below our measurement threshold of 3 to 5nm.

For high fluence illumination, the volume of fused silica isotropically decreases which results in an isotropic increase of the refractive index. However, the volume change induces mechanical strains too. The latter results in strain induced birefringence. Finite element calculations predict birefringence along a circular annulus at the boundary between the exposed and nonexposed regions. This can be seen in Fig. 10. For low level exposure no real volume change occurs, therefore no strain induced birefringence can be observed. However, the refractive index still decreases due to an as yet unknown process.

The scaling laws of compaction are known: it is a quadratic function of the intensity, and scales with the square root of the dose. The scaling laws of rarefaction are not yet known. Currently, a 20 billion shot test is in progress to determine the intensity and dose scaling law in the 0.4-0 to $0.01\ mJ/cm^2$ fluence range. We hope to see the transition from rarefication to compaction and the unambiguous simultaneous existence of the two phenomena.

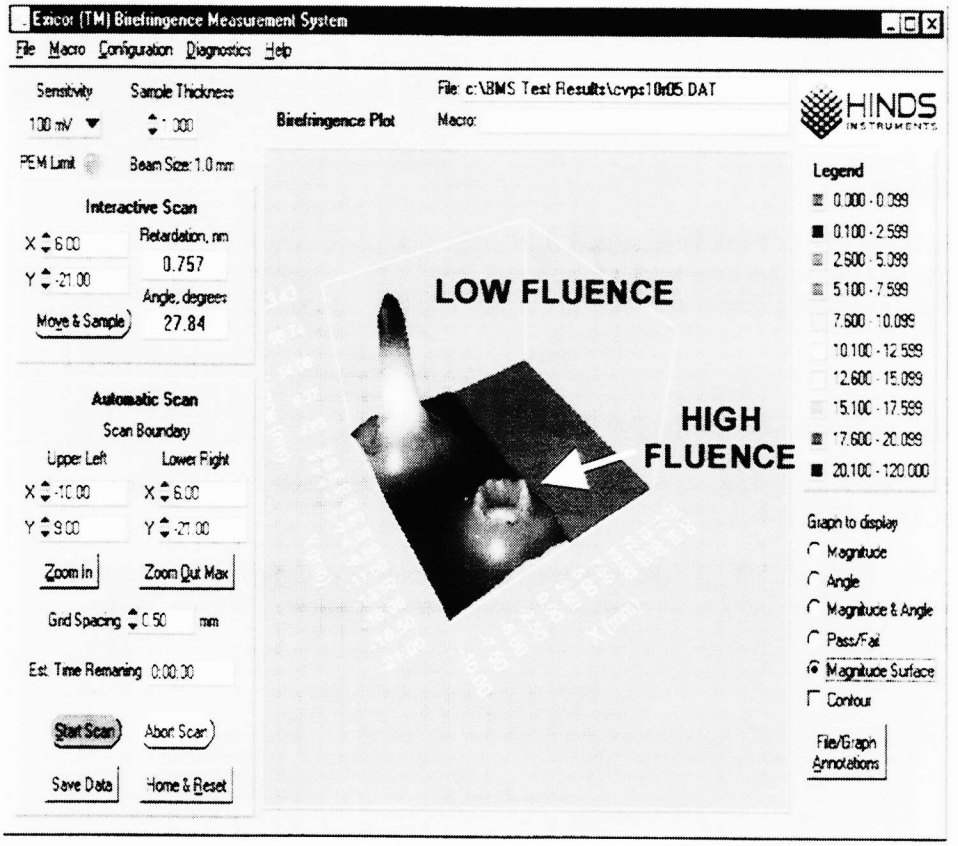

Figure 11. Sample #10 birefringence.

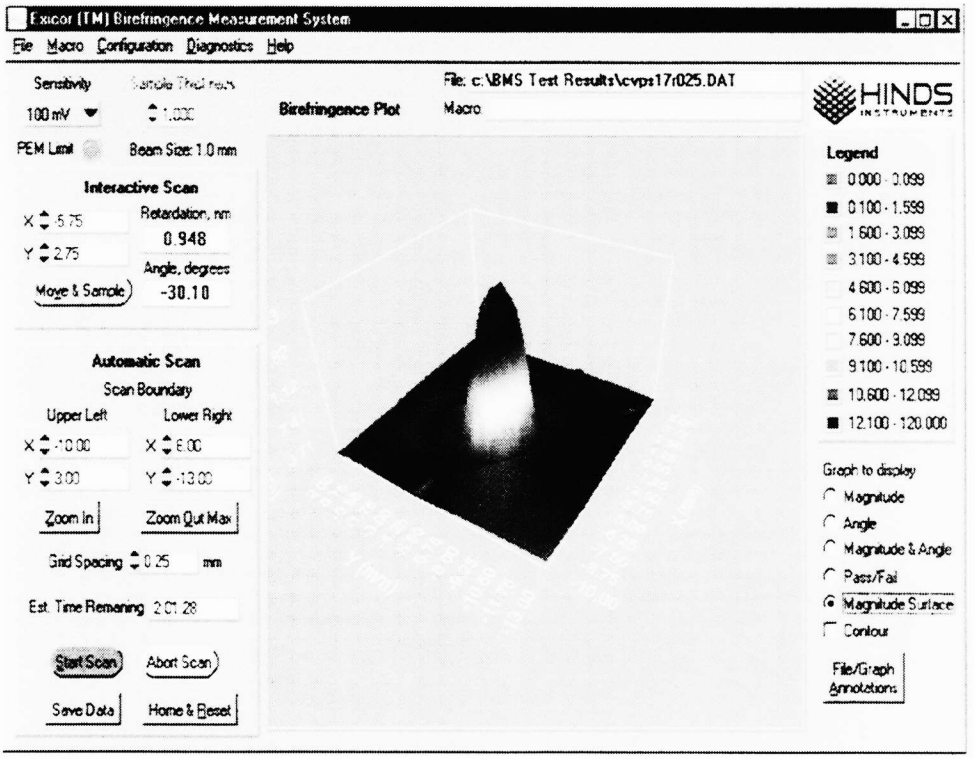

Figure 12. Sample #17 birefringence.

COMMENT

An old reference[2] which was brought to Cymer's attention by Sematech does describe "de-compaction" of fused silica by gamma rays when the silica is comparatively hydrogen-rich."

Acknowledgements

The authors would like to thank International SEMATECH for their contributions to the financial support of this study. In addition the hard work of engineers James Carmichael and Todd Embree in keeping the exposure facility operating greater than 80% of the time is greatly appreciated.

References

1. See Sematech Phase 1,2,3 Compaction Study Final Reports.

2. "Radiation effects in hydrogen-impregnated vitreous silica"; J.E. Shelby; Sandia Laboratories J. Appl. Phys. 50 (5) May,1979

3. D.C. Allan, C. Smith, N.F. Borelli, Measurement and analysis of compaction in fused silica, Symposium on Laser-Induced Damage in Optical Materials Boulder, Colorado, 1998, p 16-27.